CRYSTAL GROWTH & DESIGN

Article

pubs.acs.org/crystal

Influence of Batch Cooling Crystallization on Mannitol Physical Properties and Drug Dispersion from Dry Powder Inhalers

Waseem Kaialy,*[,†,‡] Hassan Larhrib,[§] Martyn Ticehurst,[⊥] and Ali Nokhodchi*[,†]

[†]Chemistry and Drug Delivery Group, Medway School of Pharmacy, University of Kent, ME4 4TB, Kent, U.K.

[‡]Pharmaceutics and Pharmaceutical Technology Department, University of Damascus, Damascus 30621, Syria

[§]Faculty of Applied Sciences, University of Huddersfield, Huddersfield, West Yorkshire, U.K.

[⊥]Pharmaceutical Sciences Pfizer Ltd, Ramsgate Road, Sandwich, Kent CT13 9NJ, U.K.

Supporting Information

ABSTRACT: This study provides, for the first time, an evaluation of the physicochemical properties of batch cooling crystallized mannitol particles combined with how these properties correlated with the inhalation performance from a dry powder inhaler (Aerolizer). The results showed that the type of polymorph changed from β-form (commercial mannitol) to mixtures of β- + δ-mannitol (cooling crystallized mannitol crystals). In comparison to mannitol particles, crystallized at a higher supersaturation degree, a lower degree of supersaturation favored the formation of mannitol crystals with a more regular and elongated habit, smoother surface, higher specific surface area, higher fine particle content, higher bulk density, and higher tap density. Cooling crystallized mannitol particles demonstrated considerably lower salbutamol sulfate−mannitol adhesion in comparison to commercial mannitol, with a linear reduction as surface roughness decreased and fines content increased. Also, mannitol crystals with smoother surfaces demonstrated a reduction in salbutamol sulfate content uniformity (expressed as %CV) within salbutamol sulfate−mannitol formulations. Despite the different physical properties, all mannitol products showed similar flow properties and similar emission of salbutamol sulfate upon inhalation. However, mannitol crystals grown from lower supersaturation (reduced roughness and increased fines) generated a finer aerodynamic size distribution and consequently deposited higher amounts of salbutamol sulfate on lower stages of the impactor. Regression analysis indicated linear relationships showing higher fine particle fraction of salbutamol sulfate in the case of mannitol particles having a more elongated shape, higher fines content, higher specific surface area, higher bulk density, and higher tap density. In conclusion, a cooling crystallization technique could be controlled to produce mannitol particles with controlled physical properties that could be used to influence aerosolization performance of a dry powder inhaler product.

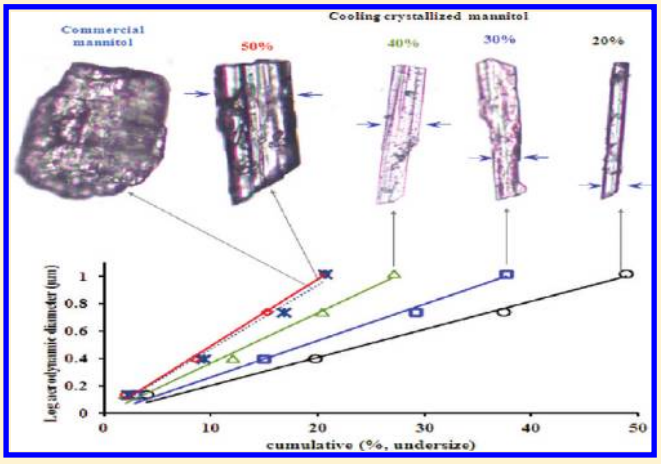

1. INTRODUCTION

Drug administration to the respiratory tract is one of the oldest drug delivery routes.[1] Dry powder inhalers (DPIs) are products that employ both powder technology and device technology. DPIs are considered attractive delivery devices due to their several advantages. They are reasonably stable,[2] environmentally friendly, easy to formulate compared to pressurized metered dose inhalers, and have a good potential for systemic drug delivery.[3,4] However, despite its widespread use, high drug delivery efficiency to the lungs is still a major challenge for DPI formulations.[5−7] Therefore, there is increased need for DPI formulations with improved dispersion and aerosolization properties.

It is well documented that DPI performance is dependent on both physical properties of drug particles and carrier particles. For example, it has been shown that higher amounts of drug could be delivered to lower airway regions by decreasing the mean size of either drug particles[8] or carrier particles.[9,10] The presence of fine particles on the carrier surface has improved the inhalation performance of DPI formulations by decreasing the drug-carrier contact area and consequently reducing drug-carrier adhesion forces.[7,11] Surface morphology of carrier particles has been modified in order to obtain improved drug dispersion properties, where smoother surface[6,12] or higher specific surface area[12,13] produced a higher fine particle fraction of drug. Manipulating particle shape, for example, elongated drug particles[14] or elongated carrier particles,[15] can be used to enhance particle deposition profiles in the respiratory airways.

Received: February 15, 2012
Revised: May 2, 2012
Published: May 10, 2012

Finally, a number of publications have demonstrated that DPI formulation performance is dependent on drug−drug cohesive forces and drug-carrier adhesive forces, described as cohesive−adhesive balance (CAB) (e.g., ref 16).

Mannitol demonstrated promising properties for inhalation drug delivery through DPIs.[6,12] However, little attention has been paid to mannitol as a potential carrier for DPI formulations. The aim of the present study was to provide, for the first time, a systemic evaluation of the effect of batch cooling crystallization (which is a widely used technique for the production of high-value chemicals)[17] on the physicochemical properties and aerosolization performance of mannitol. Different crystallized mannitol powders were prepared and then characterized in terms of physicochemical properties and in vitro DPI aerosolization performance. By comparing different mannitol powders, it is possible to evaluate the influence of mannitol physical properties on drug inhalation behavior from dry powder inhalers.

2. EXPERIMENTAL SECTION

2.1. Materials. D-Mannitol and micronized salbutamol sulfate (SS) [$D_{50\%}$ = 1.66 ± 0.06 μm and $D_{90\%}$ = 3.14 ± 0.31 μm][10] were obtained from Fisher Scientific, U.K., and LB Bohle, Germany, respectively.

2.2. Preparation of Cooling Crystallized Mannitol Powders. Supersaturated aqueous solutions of mannitol were prepared at different concentrations: 20, 30, 40, and 50% w/v, respectively. To this end, different amounts of mannitol 5, 7.5, 10, and 12.5 g were dissolved in deionized water under stirring (250 rpm) at 30, 47, 57, and 65 °C, respectively, such that the final volume solution reaches 25 mL. After being completely dissolved, all solutions were removed from heating and allowed to settle and cool (uncovered) at ambient conditions (20 °C, 50% RH) for 96 h (after 96 h no apparent water could be observed in crystallization media of any samples). Then, each crystallized mannitol (CrM) powder was harvested and left to dry in an oven at 60 °C for 24 h. After that, CrM powders were transferred separately into sealed glass vials until required. For comparison purposes, commercial mannitol (CM) was used as a control in this study. In this study, supersaturation was expressed as absolute supersaturation ($\Delta C = C/C_0$) where C is the concentration of the dissolved mannitol at a given temperature and C_0 is the saturation concentration.

2.3. Selection of Mannitol Particle Size Fraction. Prior to any investigation, in order to minimize the effect of particle size, all mannitol powders were mechanically sieved (Endecotts Ltd., England mechanical shaker and Retsch Gmbh Test Sieve, Germany) for 15 min to collect 63−90 μm size fractions.[6]

2.4. Fourier Transform Infrared Spectroscopy (FT-IR). FT-IR spectra (FT-IR equipment: Perkin-Elmer, USA) were used to investigate any possible changes in crystallized mannitol that may have occurred at the molecular level during the crystallization or drying processes. The scanning range was 450−4000 cm^{-1} and the resolution was 1 cm^{-1}.

2.5. Differential Scanning Calorimetry (DSC). A differential scanning calorimeter (DSC7, Mettler Toledo, Switzerland) was used to characterize DSC traces of all mannitol samples. Samples (4−5 mg) were heated from 25 to 300 °C in aluminum pans. A purge gas of nitrogen was passed over the pans with a flow rate of 50 mL/min. In order to obtain better detection of mannitol polymorphic form, several heating rates were applied (3 °C/min, 10 °C/min, and 30 °C/min). Melting points and enthalpies were calculated by the software.

2.6. X-ray Powder Diffraction (XRPD). X-ray diffractometry of the commercial mannitol and all recrystallized mannitol were performed using a Siemens diffractometer (Siemens, D5000, Germany). The cross-section of samples were exposed to X-ray radiations (Cu Kα) with a wavelength of 1.5406 Å. Samples were placed into a stainless steel holder and the surface of powder was leveled manually for analysis. The sample was scanned between 5° and 40° of 2θ with a step size of 0.019° and a step time of 32.5 s.

2.7. Laser Diffraction and Image Analysis Optical Microscopy. Particle size analysis was conducted using a Sympatec (Clausthal-Zellerfeld, Germany) laser diffraction particle size analyzer as described elsewhere.[12] In addition, quantitative size and shape optical image analysis were performed using a computerized morphometric analyzing system (Leica Q Win Standard Analyzing Software and Leica DMLA Microscope; Leica Microsystems Wetzlar GmbH, Wetzlar, Germany). For each mannitol sample, a small amount of powder (about 20 mg) was homogenously scattered onto a microscope slide and a minimum of 3000 particles were detected and measured. Several shape descriptors were employed including aspect ratio (AR) (eq 1), flatness ratio (FR) (eq 2), roundness (eq 3), and roughness (eq 4):[18]

$$\mathrm{AR} = \frac{\text{length}}{\text{width}} \tag{1}$$

$$\mathrm{FR} = \frac{\text{breadth}}{\text{thickness}} \tag{2}$$

$$\text{roundness} = \frac{\text{perimeter}^2 \times 1000}{4 \times P \times \text{area}} \tag{3}$$

$$\text{roughness} = \frac{\text{perimeter}}{\text{ConvxPerim}} \tag{4}$$

2.8. Scanning Electron Microscopy (SEM). Electron micrographs of mannitol, salbutamol sulfate (SS), and mannitol-SS samples were obtained using a scanning electron microscope (Philips XL 20, Eindhoven, Netherlands) operating at 15 kV. Prior to observation, the specimens were mounted on a metal stub with double-sided adhesive tape and coated under a vacuum with gold in an argon atmosphere.

2.9. Density and Powder Flow Measurements. True density (D_{true}), bulk density (D_{bulk}), tap density (D_{tap}), Carr's index (CI), Hausner ratio (HR), and porosity for all mannitol samples were measured as described in detail elsewhere.[7] As using only one method to measure flowability might give poor estimations,[19] flowability for all mannitol powders was further assessed by measuring the angle of repose (α). A pile was built by dropping 1 g of each mannitol powder through a 75 mm flask on a flat surface. The height between the base where the powder has been poured and the funnel tip was 3 cm. Then, the angle of repose (α) was calculated using eq 5, where h is the height of the powder cone and D is the diameter of the base of the formed powder pile:

$$\tan \alpha = \frac{2h}{D} \tag{5}$$

2.10. In Vitro Formulation Evaluations. *2.10.1. Preparing Drug-Carrier Formulations.* All mannitol samples were blended with SS in a ratio of 67.5:1 (w/w) in an aluminum container. This blending was carried out using a Turbula mixer (Willy A. Bachofen AG, Maschinenfabrik, Basel, Switzerland) at a constant speed of 100 rpm for 30 min.

2.10.2. Evaluation of Drug-Carrier Adhesion Forces. Air depression sieving was employed to assess drug-carrier adhesion forces. An air jet sieving machine (Copley Scientific, Nottingham, UK) was operated at a volume flow that generates negative pressure of 4 KPa. Each formulation (1 g) was placed on top of the 45 μm sieve (Retsch GmbhTest Sieve, Germany), and four samples (weighing 33 ± 1.5 mg corresponding to unite SS dose: 481 ± 22 μg) were removed from different areas of each formulation after different functional sieving times (5, 25, 60, and 180 s). Drug content in each sample was quantified using the HPLC method as previously described.[6] Adhesion assessments were conducted in an air-conditioned laboratory (20 °C, 50% RH).

2.10.3. Homogeneity Test. After blending, a minimum of five randomly selected samples from different positions of formulation powder bed were taken for assay of SS content. Each sample, weighing 33 ± 1.5 mg, was dissolved in 100 mL of distilled water in a volumetric

dx.doi.org/10.1021/cg300224w | Cryst. Growth Des. 2012, 12, 3006−3017

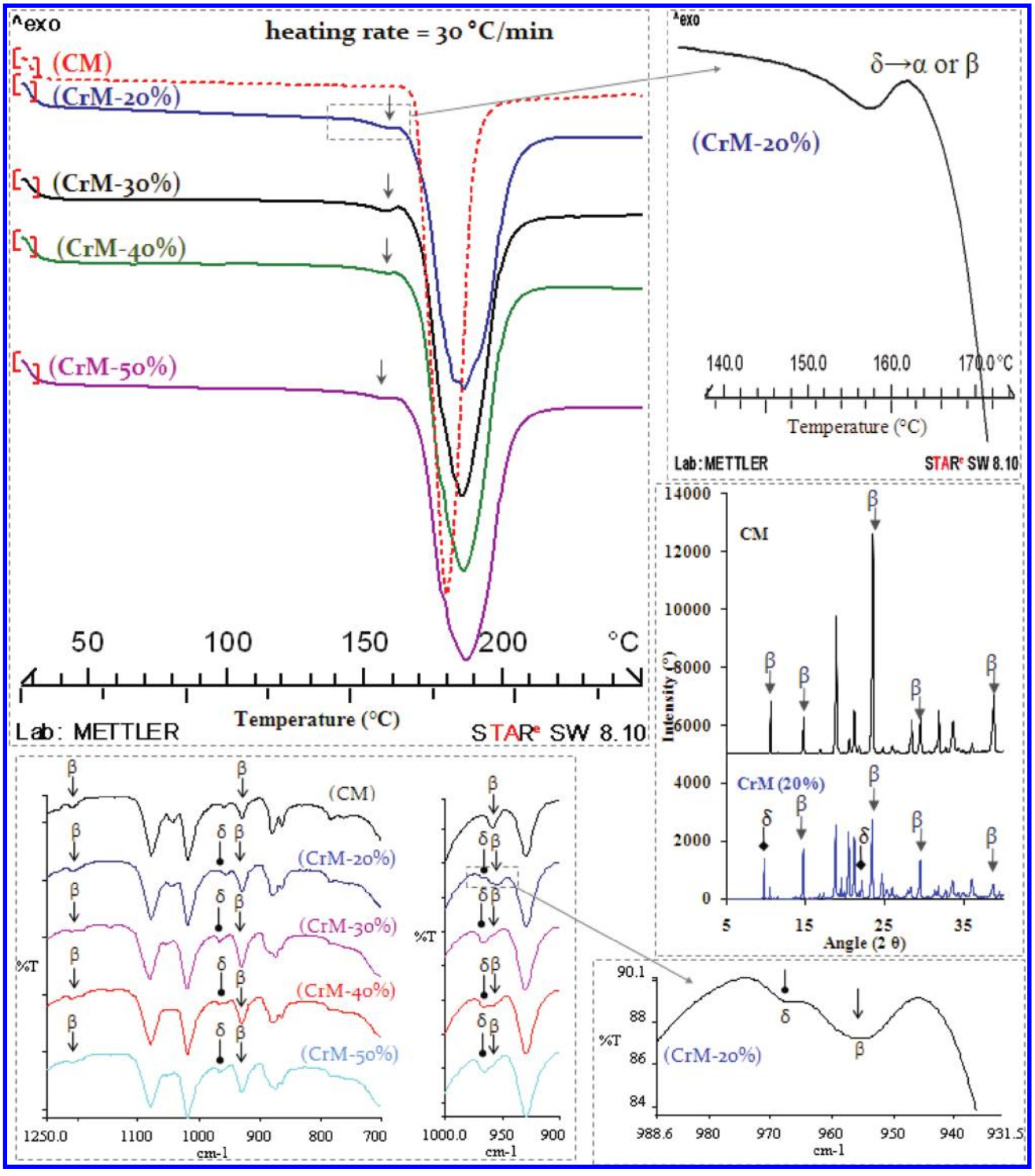

Figure 1. DSC traces, FT-IR spectra, and/or PXRD patterns for commercial mannitol (CM) and cooling crystallized mannitol (CrM) from 20%, 30%, 40%, and 50% w/v solutions.

flask and the amount of SS was determined using HPLC. For each formulation, average drug content (% potency, nominal SS dose) was calculated and drug content homogeneity was expressed as percentage coefficient of variation (% CV).

2.10.4. In Vitro Deposition Study. After blending, each formulation was filled manually in hard gelatin capsules (size 3) such that each capsule contained 33 ± 1.5 mg of formulation corresponding to 481 ± 22 μg of SS, which was the same dose as in commercially available Ventolin Rotacaps. After filling, capsules were stored for equilibration in sealed glass vials at ambient conditions (20 °C, 50% RH) for at least 24 h prior to investigation. Pulmonary drug deposition profiles of different formulations were assessed in vitro using a multi stage liquid impinger (MSLI) equipped with a USP induction port (Copley Scientific, Nottingham, UK) at a flow rate of 92 L/min as explained in detail elsewhere.[6] Each deposition experiment involved the actuation of 10 capsules and was repeated a minimum of three times. Several parameters were employed to characterize deposition profiles for all formulations under investigation,[6] including percent emission (EM), impaction loss (IL), mass median aerodynamic diameter (MMAD), and geometric standard deviation (GSD). Fine particle dose

dx.doi.org/10.1021/cg300224w | Cryst. Growth Des. 2012, 12, 3006−3017

($FPD_{\leq 5\ \mu m}$) was calculated by interpolation of drug aerodynamic size distributions obtained by MSLI deposition profiles. $FPF_{\leq 5\ \mu m}$ was calculated as the percent ratio of $FPD_{\leq 5\ \mu m}$ to RD. Effective inhalation index (EI) and theoretical aerodynamic diameter (D_{ae}) were calculated using eqs 6 and 7 respectively[10] (where D_e is geometric mean diameter, ρ is true density, and x is the dynamic shape factor for nonspherical particles which could be assumed as 1):

$$EI = (EM \times FPF_{\leq 5\mu m})^{1/2} \quad (6)$$

$$D_{ae} = D_e \times \sqrt{\frac{\rho}{x}} \quad (7)$$

2.11. Statistical Analysis. One-way analysis of variance (ANOVA) was applied (where appropriate) to compare results in this study. P values less than 0.05 were considered as indicative of statistically significant difference.

3. RESULTS AND DISCUSSION

3.1. Crystallization Procedure. The crystal physical properties are profoundly influenced by rate of crystallization which is mainly governed by supersaturation.[20] The effect of absolute supersaturation (which is 3, 13, 23, and 33 for mannitol crystallized from 20%, 30%, 40%, and 50% (w/v) solutions, respectively) on cooling crystallized mannitol (CrM) particle properties was studied (the saturated mannitol concentration was 17% w/v at 21 °C). Following preparation of all mannitol saturated solutions, none of the CrM particles could be observed immediately in the crystallization media. In fact, slow crystallization rate is the main disadvantage of cooling crystallization technique,[21] due to the large width of metastable zone. Nevertheless, slow cooling is advantageous in terms of attaining maximum product yield, minimum agglomeration,[22] fewer defects in the crystal lattice,[23] and improved product purity.[24] As the supersaturation increases induction time (defined as the time elapsing between cooling and the formation of detectable crystals) decreases whereas mannitol crystal growth rate increases. For each medium, the longer the mannitol supersaturated solutions were kept the greater the amounts of crystals were observed to form at the expense of water amounts. No water could be visualized in the crystallization media after 24 h in the case of 33 and 23 absolute supersaturations, but it was after 96 h in the case of 13 and 33 absolute supersaturations. Crystal yields were high and did not show significant differences due to supersaturation degree (97− 98%).

3.2. Solid State Characterization. At slow heating rates (3 and 10 °C/min), all mannitol samples showed similar DSC trances having one endothermic transition around 167 ± 1 °C (representing melting of either α-mannitol or β-mannitol which are not distinguishable from each other by DSC).[25] However, FT-IR spectra of commercial mannitol (CM) exhibited the spectrum of the reference β-mannitol pointed out in previous studies,[26] having the specific diagnostic bands at 929, 959, and 1209 cm^{-1} (Figure 1). FT-IR of CrM products exhibited both β-mannitol diagnostic bands and delta mannitol (δ-mannitol) diagnostic band at 967 cm^{-1},[26,12] indicating the presence of both β-mannitol and δ-mannitol (Figure 1).

At higher heating rates (30 °C/min), DSC traces of CrM samples displayed two-phase transitions (Figure 1). The first transition is characterized by an endothermic event at 157 °C, which could be related to melting of δ-mannitol,[26,12] followed by conversion of δ-mannitol form (enantiotropic toward α- and β-) to either β-mannitol form (monotropic toward α-) or α-mannitol form (Figure 1). Comparing δ-mannitol melting enthalpies of all mannitol samples suggested that mannitol crystallized from lower concentrations contained a higher quantity of δ-mannitol. The second transition corresponds to the melting of either α-mannitol or β-mannitol phase (Figure 1). The FT-IR and DSC results obtained for CM was supported by the PXRD pattern of CM (Figure 1). The PXRD pattern corresponds to that of β-mannitol form with its diagnostic peaks at 10.56°, 14.71°, 23.4°, 29.5°, and 38.8°.[26] The PXRD pattern of CrM-20% exhibited both β-mannitol diagnostic peaks and δ-mannitol diagnostic peaks at 9.74° and 22.2°,[15,26] confirming the presence of both β-mannitol and δ-mannitol (Figure 1). In conclusion, CM was pure β-mannitol whereas CrM particles crystallized as mixtures of β-mannitol and δ-mannitol. However, the presence of δ-mannitol within CrM samples could not be detected by DSC running at slow heating rates. Both β- and δ-mannitol forms are known to be chemically or physically stable for at least 5 years in dry atmosphere (25 °C). δ-Mannitol has a different structure to β-mannitol and would be expected to have different preferred morphology and surface properties as discussed in the Particle Shape Analysis section of the article.

3.3. Particle Size Measurements. Although all mannitol samples were carefully sieved in an identical method, CrM powders showed smaller PSDs (Figure 2a), higher fine particle

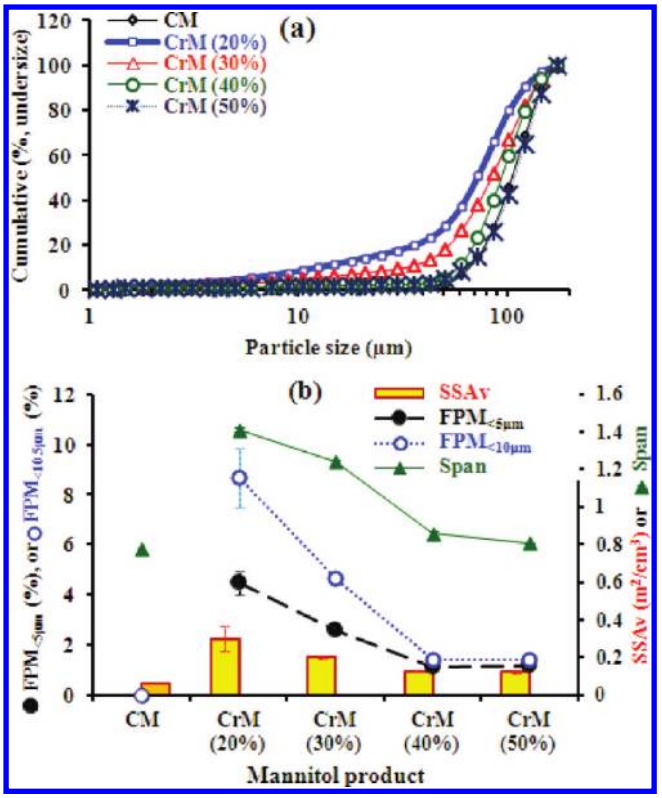

Figure 2. Cumulative particle size distribution (a); (yellow bars) volume specific surface area (SSA_v), fine mannitol particles (●) less than 5 μm ($FPM_{<5\ \mu m}$) or (○) less than 10 μm ($FPM_{<10\ \mu m}$), and (▲) span (b) for different 63−90 μm sieved mannitol samples: commercial mannitol (CM) and cooling crystallized mannitol (CrM) from 20%, 30%, 40%, and 50% (w/v) solutions (mean ± SD, n = 5).

mannitol content ($FPM_{<5\ \mu m}$ and $FPM_{<10\ \mu m}$), higher volume specific surface area (SSA_v), and higher span than CM (Figure 2b). This could be attributed to variations between different mannitol products in terms of crystal habits as shown later.

dx.doi.org/10.1021/cg300224w | Cryst. Growth Des. 2012, 12, 3006−3017

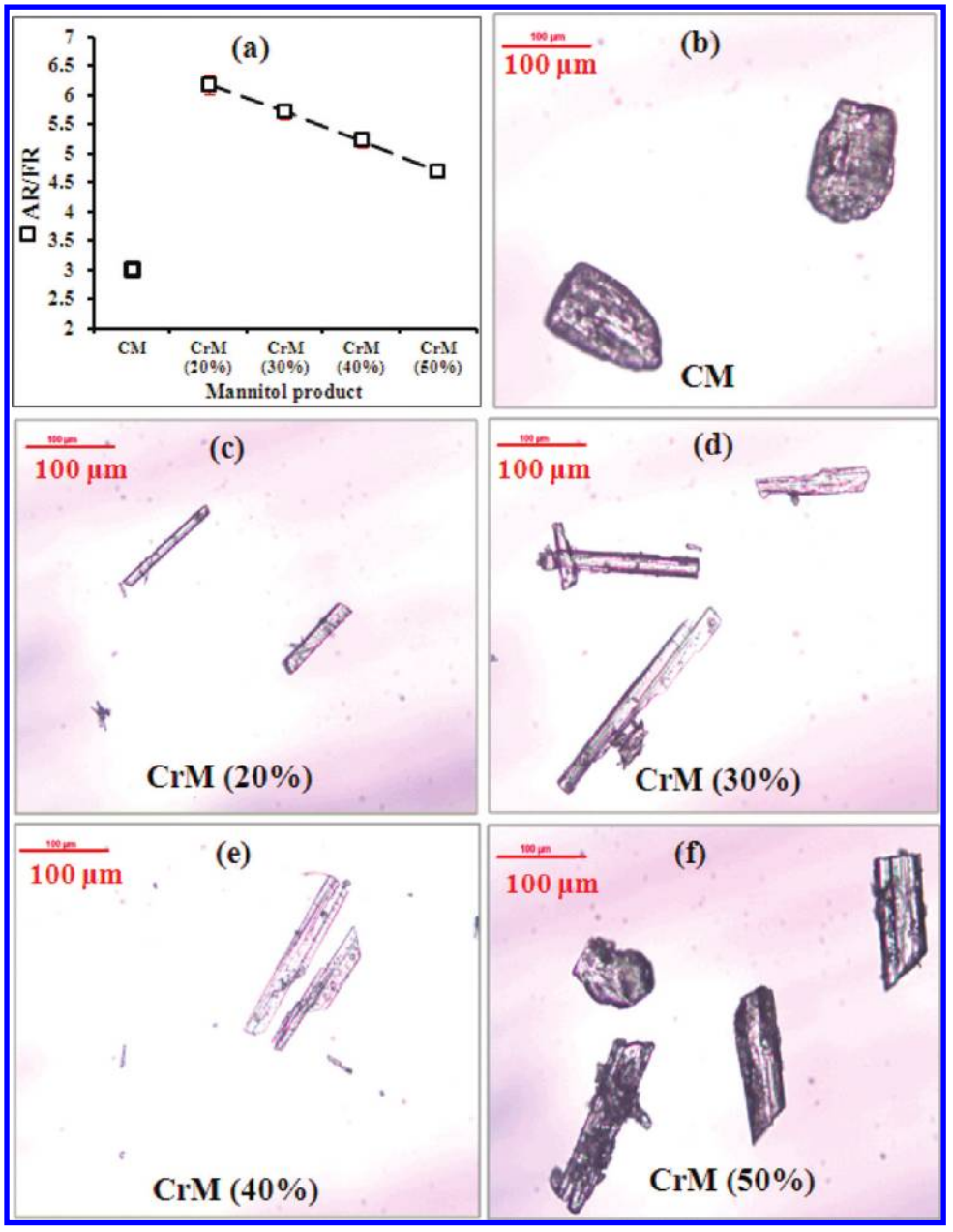

Figure 3. (a) Aspect ratio/flatness ratio (AR/FR) (□), and representative microscope images, for different 63−90 μm sieved mannitol powders: commercial mannitol (CM) (b) and cooling crystallized mannitol (CrM) from 20% (c), 30% (d), 40% (e), and 50% (w/v) (f) solutions.

Generally, mannitol crystals grown from lower supersaturations demonstrated higher $FPM_{<5\ \mu m}$, higher $FPM_{<10\ \mu m}$, and higher SSA_v (Figure 2b). This could be attributed to a possible increased number of particle agglomerates with increasing supersaturation (due to increased nucleation rates).

Statistical analysis on all mannitol samples showed that SSA_v has a high correlation with VMD (−0.95), $FPM_{<5\ \mu m}$ (1.00), $FPM_{<10\ \mu m}$ (0.99), and span (0.96) confirming a higher SSA_v for mannitol particles with smaller VMD, higher FPM content, and higher span. Mannitol powders crystallized from higher supersaturations have narrower (more homogeneous) size distributions as indicated by a smaller span (Figure 2b). This was in agreement with previous studies[27,28] and could be attributed to increased driving forces of nucleation in the case of solutions with higher supersaturations.

3.4. Particle Shape Characterization. Representative microscopic images and SEM photographs for all mannitol powders inspected in this study are shown in Figures 3 and 4, respectively. It can be observed that particle shape and surface topography of different mannitol powders varied considerably (Figures 3 and 4). In fact, as the crystallization rate in the vicinity of the growing crystal surfaces is dependent on the degree of supersaturation, any change of supersaturation is expected to have an effect on the crystal morphology. These differences in carrier particle morphology are anticipated to have a significant effect on DPI performance.[15]

Aspect ratio (AR) and flatness ratio (FR) are the fundamental first-order descriptors of particle form. AR/FR is a shape descriptor helpful to describe the overall particle shape. All CrM particles showed higher AR/FR than CM (Figure 3a), indicating that CrM particles have more elongated habit. This might be related to the presence of δ-mannitol within CrM particles (Figure 1) as δ-mannitol crystals have elongated (oblong) unit cell and crystal habit.[29] This was further

dx.doi.org/10.1021/cg300224w | Cryst. Growth Des. 2012, 12, 3006−3017

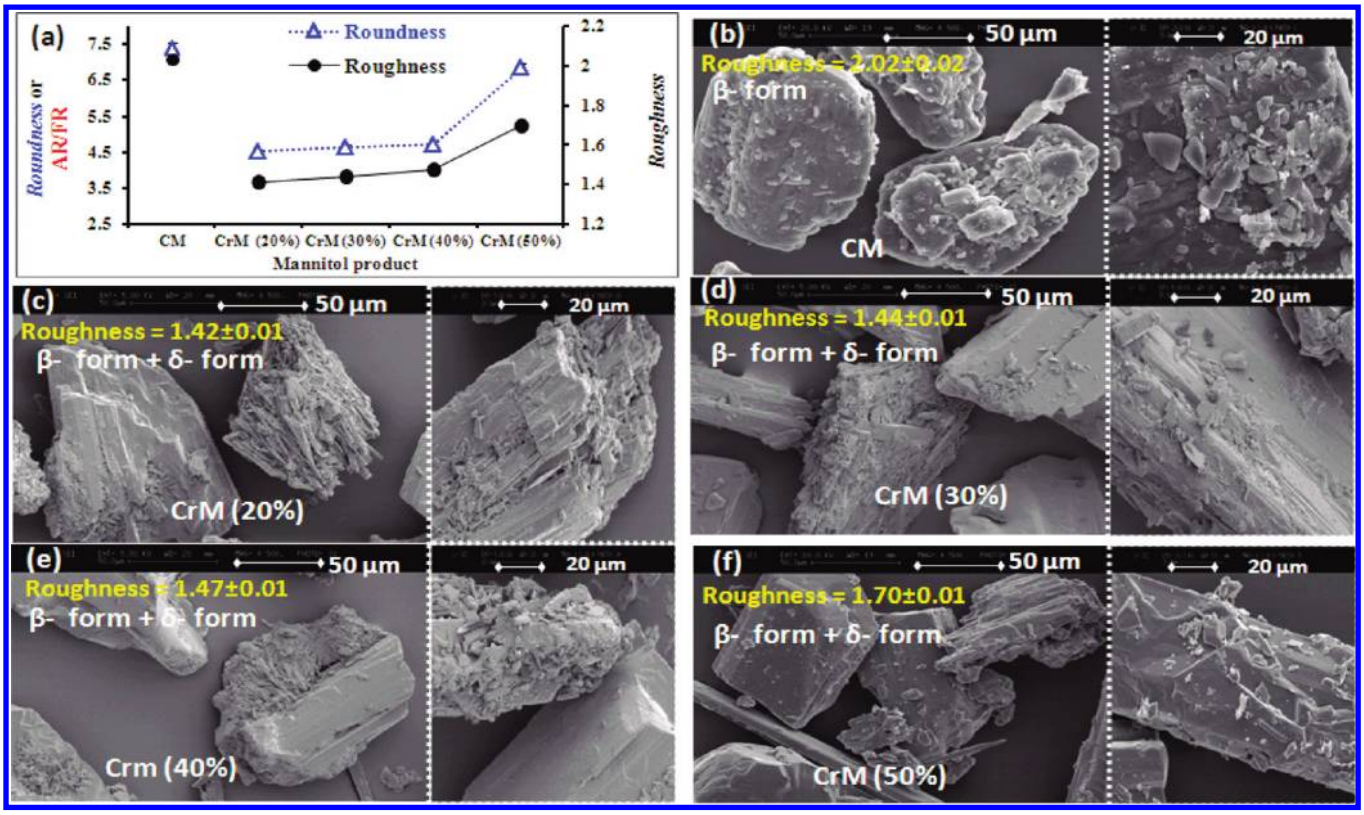

Figure 4. (a) (Δ) Roundness, (●) roughness; SEM images of different 63−90 μm sieved mannitol powders: commercial mannitol (CM) (b) and cooling crystallized mannitol (CrM) from 20% (c), 30% (d), 40% (e), and 50% (w/v) (f) solutions.

supported by representative microscope images (Figure 3b−f) and SEM photographs (Figure 4b−f). Comparing AR/FR values of all CrM particles showed that there was a linear inverse relationship between AR/FR values and mannitol supersaturation degree (linear, r^2 = 1, AR/FR = −0.0498 supersaturation +7.2008) (Figure 3a). This demonstrates that a low degree of mannitol supersaturation favored the formation of needle-shaped crystals, whereas a high degree of supersaturation favored the formation of flat shaped-crystals. This could be attributed to the fact that the effect of supersaturation on growth kinetics is different for each crystallographic face.[30] At low supersaturation, crystal growth of mannitol by hydrogen bonding is expected to be favored in one direction ("preferred" axis which has the highest free hydrophilic groups) leading to the formation of more elongated crystals (δ-mannitol). However, at high supersaturation, secondary nucleation might become more dominant on crystal faces to the "preferred" axis restraining any further primary growth along this axis and as a result mannitol crystal elongation decreases as supersaturation increases.

Roundness is a second-order shape descriptor reflecting variations at particle corners, whereas roughness is a third-order shape property independent of both first-order (e.g., AR and FR) and second-order (e.g., roundness) shape descriptors. CrM particles showed smaller roundness and smaller roughness than CM (Figure 4a), which is indicative of their more regular shape and smoother surface texture. Mannitol crystals grown from lower supersaturations have smaller roundness and smaller roughness indicating their more regular shape and smoother surface topography (Figure 4a). This was further supported by SEM photographs where, unlike CM (in which large protuberances could be observed forming angular edges (Figure 4b)), CrM particles have subrounded-subangular shape (Figure 4c−f). Moreover, visualization of surface topography demonstrated that CM has a wrinkled fractured surface with a higher degree of roughness (Figure 4b), whereas CrM particles have a relatively smoother surface with less irregularities (Figure 4c to 3f).

The mechanism of crystal growth is dependent on the degree of supersaturation. For example, spiral growth theory is more relevant to the crystal growth from low supersaturations,[31] whereas classical crystal growth theory might happen for the crystal growing from high supersaturations.[32] At lower levels of supersaturation, kinetics of crystallization becomes slow and this favors ordered (regular) crystal growth patterns, small surface nuclei, and perfect lattice on crystal surface, generating crystals with regular shape and smoother surface. On the contrary, higher supersaturation induces accelerated nucleation (by lowering the interfacial energy in the solid-solution interface) and secondary (heterogeneous) nucleation growth, which generate crystals with less regular shape and rougher surfaces. In conclusion, crystal habit is profoundly influenced by the rate of crystallization. Mannitol crystals grown from lower supersaturations have a more regular shape, more elongated shape, and smoother surface topography. CM particles showed the roughest surface topography and the lowest degree of shape regularity and shape elongation.

3.5. Density and Flowability Assessments. All CrM particles showed considerably smaller D_{true} than CM (1.48 ± 0.01 g/cm^3 versus 1.52 ± 0.00 g/cm^3), suggesting that δ-mannitol might have smaller D_{true} than β-mannitol. Also, CrM particles demonstrated smaller D_{bulk}, and smaller D_{tap} than CM (Figure 5). Mannitol powders crystallized from higher supersaturations demonstrated smaller D_{bulk} (linear, r^2 =

dx.doi.org/10.1021/cg300224w | Cryst. Growth Des. 2012, 12, 3006−3017

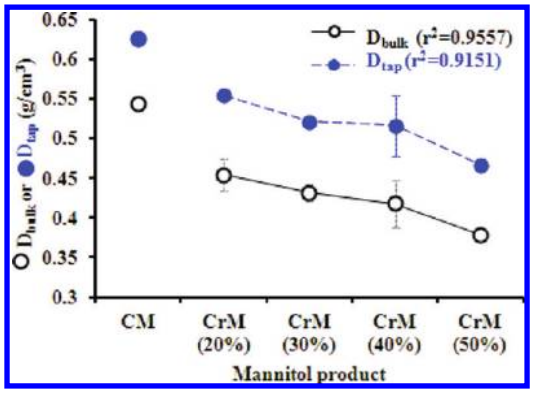

Figure 5. (○) Bulk density (D_{bulk}) and (●) tap density (D_{tap}) for different 63−90 μm sieved mannitol powders: commercial mannitol (CM) and cooling crystallized mannitol (CrM) from 20%, 30%, 40%, and 50% (w/v) solutions (mean ± SD, $n \geq 5$).

0.9557) and smaller D_{tap} (linear, r^2 = 0.9151) (Figure 5). Conversely, porosity obtained for CrM powders was higher than CM (69.4−74.6% versus 64.2%), and mannitol powders crystallized from higher supersaturations showed higher porosity (linear, r^2 = 0.9368, figure not shown). This indicates increased interparticulate cohesive forces for CrM particles with increasing supersaturation.

Unlike D_{true} (particle characteristic), D_{bulk}, D_{tap}, and porosity are powder characteristics related to spaces and voids within the powder. Lower porosity, higher D_{bulk}, and higher D_{tap} for mannitol powders crystallized from lower supersaturations could be attributed to a higher degree of interparticulate average contact points within the powder due to a higher content of fine particles (Figure 2b), more regular shape (smaller roundness), and smoother particle surface (Figure 4). Despite their difference in terms of density, all sieved mannitol powders showed statistically similar CI (16.0 ± 2.2% − 19.0 ± 2.5%), similar HR (1.15 ± 0.01 − 1.23 ± 0.02), and similar α (35.2 ± 4.8° − 40.3 ± 5.2°) corresponding to good to fair flow properties.

3.6. DPI Formulation Assessments. *3.6.1. SS-Mannitol Formulation Evaluation by SEM.* SEM photographs of SS and all SS-mannitol formulations are shown in Figure 6. SEM images of SS particles (Figure 6a) were observed to be less than 5 μm in size exhibiting a high degree of agglomeration and the typical rectangular (or rod) shape pointed out in previous studies.[13] In the case of SS-mannitol formulations (Figure 6b−f), SS particles could be morphologically detected as, generally, single (individual) particles adhered to large mannitol particle surfaces. This confirms the formation of SS-mannitol interactive ordered mixtures suitable for DPI systems. By observing surface topography, fine particles are easily visible on the surface of larger mannitol particles (Figures 6b−f), which is in agreement with PSD measurements (Figure 2). These fines correspond to "intrinsic (not added)" fine mannitol particles attached to the surface of large mannitol particles which could not be removed by sieving. Compared to SS-CM formulation, SS-CrM

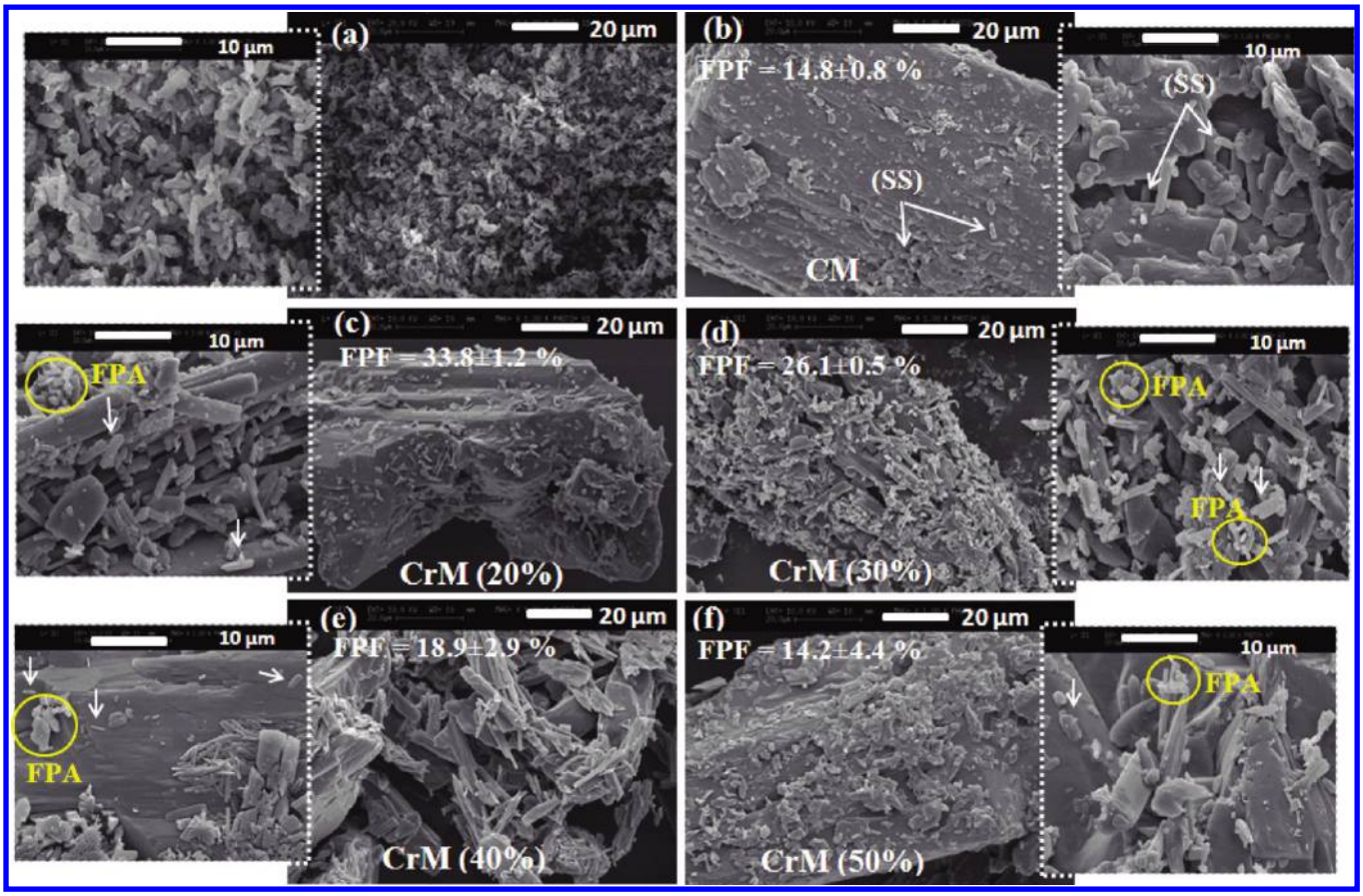

Figure 6. SEM images for micronized salbutamol sulfate alone (SS) (a), and different SS-mannitol formulations containing different 63−90 μm sieved mannitol powders: commercial mannitol (CM) (b) and cooling crystallized mannitol (CrM) from 20% (c), 30% (d), 40% (e), and 50% (w/v) (f) solutions. FPA: fine particle aggregates (SS and fine particle mannitol). Arrows indicate SS particles.

Table 1. Percent Potency and Coefficient of Variation (Mean Potency (CV)) and Percent Amounts of Salbutamol Sulphate Remained on Top of the 45 μm Sieve (mean (SD), $n \geq 3$) after Different Functional Sieving Times for DPI Formulations Containing Different 63−90 μm Sieved Mannitol Powders: Commercial Mannitol (CM) and Cooling Crystallized Mannitol (CrM) from 20%, 30%, 40%, and 50% (w/v) Solutions

	sieving time				
mannitol product	0 s: % potency(CV)	5 s	25 s	60 s	180 s
CM	93.9 (1.76)	89.7 (2.9)	78.9 (2.9)	73.2 (3.2	46.7 (2.6)
CrM-20%	76.8 (9.44)	35.5 (3.6)	13.4 (1.1)	9.9 (0.0)	9.1 (0.8)
CrM-30%	91.5 (9.36)	62.3 (6.2)	43.6 (4.3)	35.7 (0.8)	24.5 (0.4)
CrM-40%	67.6 (9.26)	67.4 (9.9)	18.2 (0.8)	12.2 (0.9)	12.6 (1.4)
CrM-50%	90.6 (6.30)	78.3 (6.7)	34.2 (4.9)	15.7 (3.1)	8.4 (0.0)

formulations exhibited a decreased number of SS particle entrapped in macroscopic depressions on the mannitol surface (Figure 6), which is likely to facilitate SS detachment from CrM surfaces during inhalation. Also, SS-fine mannitol aggregates (FPA) were observed in the case of SS-CrM formulations (Figure 6c−f). These FPA are believed to be formed at the expense of SS-mannitol interactive mixtures and are expected to improve DPI performance.

3.6.2. SS-Mannitol Adhesion Assessments. Upon air jet sieving of formulations, small SS particles are expected to detach from coarse mannitol particles. Amounts of SS remaining on top of the 45 μm sieve after subjecting all formulations to different functional sieving times are given in Table 1. For all formulations, amounts of SS decreased as sieving time increased. This confirms that all formulations were ordered mixtures. Assuming the particle adhesion force is equivalent to the particle detachment force, less amounts of SS collected from the top of the 45 μm sieve is indicative of weaker SS-mannitol adhesion. Among all formulations, the highest amounts of SS after all sieving times were obtained for SS-CM formulation, whereas the lowest amounts of SS were obtained for SS-CrM-20% formulation (Table 1). This indicates that mannitol crystals grown from lowest supersaturation generated the lowest SS-mannitol adhesion forces, whereas the highest adhesion forces were obtained in the case of CM. Less SS-mannitol adhesion could be attributed to weaker SS-mannitol physical interactions. It is known that particle surface properties affect the drug-carrier contact geometry and thus has a substantial impact on drug-carrier adhesion. Figure 7 shows that SS-mannitol adhesion forces decreases as mannitol surface

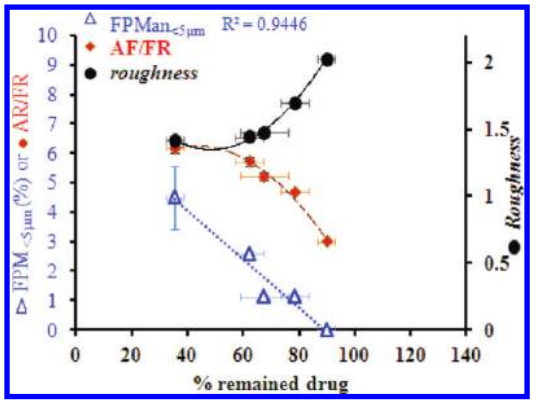

Figure 7. Percent amounts of salbutamol sulfate remaining on top of the 45 μm sieve after 5 s functional sieving time (mean ± SD, $n \geq 3$), in relation to (●) mannitol surface roughness, (♦) aspect ratio/flatness ratio (AR/FR), and (Δ) fine mannitol particles ($FPM_{<5\ \mu m}$).

smoothness, shape elongation (AR/FR), and/or fines content ($FPM_{<5\ \mu m}$) increases. This could be ascribed to entrapment of drug particles in carrier surface indentations in the case of carriers with a rougher surface.[6,12] Also, FPM on coarse mannitol surface may decrease both SS-mannitol contact area and SS-mannitol press-on adhesive forces generated during blending.

3.6.3. Formulation Homogeneity Test. Percent potency and percent CV obtained from formulations containing different mannitol powders are given in Table 1. Formulations containing CrM produced decreased potency than the CM formulation (Table 1). This could be due to reduced SS-mannitol adhesion in the case of CrM compared to CM (as proven previously), which might lead to increased amounts of "lost drug" during handling processes (e.g., mixing, storage, and capsule filling). SS-CrM formulations produced reduced drug content homogeneity than SS-CM formulation as indicated by higher % CV (Table 1). An indirect linear correlation (r^2 = 0.9952) was established between mannitol roughness and % CV of SS (Figure 8) suggesting that carriers with a rougher

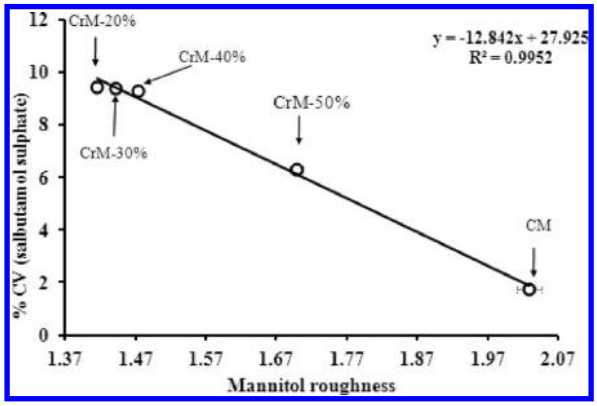

Figure 8. Relationship between mannitol surface roughness and coefficient of variation (% CV) in salbutamol sulfate content for DPI formulations containing different mannitol powders: commercial mannitol (CM) and cooling crystallized mannitol (CrM) from 20%, 30%, 40%, and 50% (w/v) solutions.

surface produce improved drug content homogeneity. Such an outcome could be explained as a higher degree of mannitol surface roughness reinforces the SS-mannitol adhesion (Figure 7).

3.6.4. In Vitro Aerosolization Studies. Mass distribution of SS deposited on I + M, IP, and different MSLI stages obtained from different formulations varied considerably for SS-mannitol formulations (Figure 9a). All CrM powders deposited higher amounts of SS on the throat (IP) (Figure 9a). Formulations

dx.doi.org/10.1021/cg300224w | Cryst. Growth Des. 2012, 12, 3006−3017

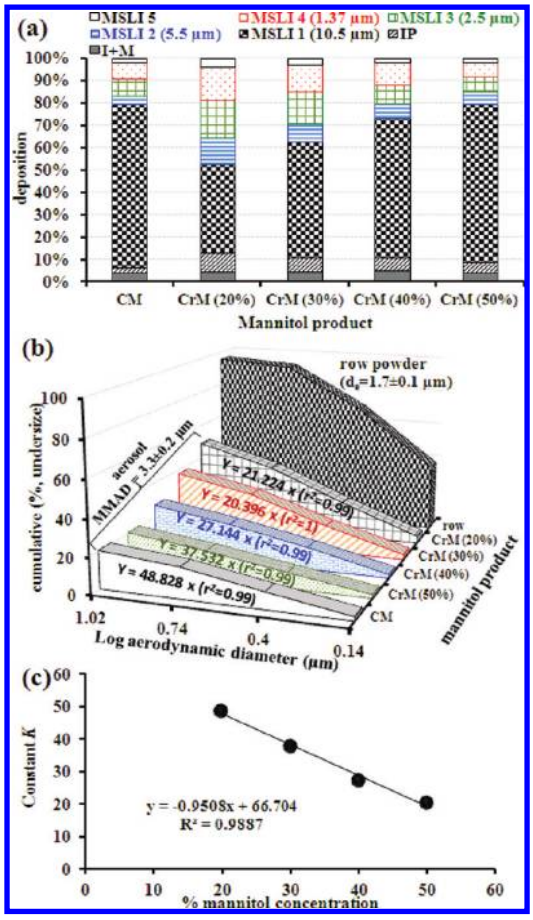

Figure 9. Mass distribution (a), aerodynamic size distribution before (solid line) and after aerosolization (b), and the relationship between constant K and mannitol concentration (c) for salbutamol sulfate when aerosolizing DPI formulations containing SS blended with different 63−90 μm sieved mannitol powders: commercial mannitol (CM) and cooling crystallized mannitol (CrM) from 20%, 30%, 40%, and 50% (w/v) solutions.

containing mannitol crystals grown from lower supersaturations deposited smaller amounts of SS on MSLI stage 1, but higher amounts on MSLI stage 2, stage 3, and stage 4 (Figure 9a). When compared with laser diffraction data, aerodynamic PSD data indicated that SS particles were not sufficiently dispersed into individual particles (Figure 9b). This could be attributed to SS particle cohesiveness and/or inadequate inhaler device dispersing efficiency to recover primary PSD of SS (which was supported by SEM images showing FPA (Figure 6c−f)). Figure 9b shows that mannitol crystals grown from lower supersaturations generated smaller aerodynamic PSDs of SS (closer to primary PSD of pure SS powder). Moreover, the slope of aerodynamic PSD curves, named as constant K,[15] which apparently reflects the tendency of SS particles to penetrate deeper into lower lung airways, was a linear function (r^2 = 0.9887) to mannitol concentration used during crystallization (Figure 9c). Such data indicate that mannitol crystals grown from lower supersaturations deliver higher amounts of SS to lower airways, indicating their preferred aerodynamic properties since β-receptors are mainly located in the lower airway regions.[33]

However, all formulations demonstrated similar (P > 0.05) MMAD (3.0 ± 0.2 - 3.4 ± 0.2 μm, $n \geq 3$) and similar GSD (2.11 ± 0.04 − 2.18 ± 0.03, $n \geq 3$) of SS. This confirms that drug aerosolization performance could not be predicted, necessarily, from MMAD and GSD alone. Moreover, this indicates a similar degree of SS agglomeration within all formulations, suggesting variations of SS inhalation behavior between different formulations could be attributed to different SS-mannitol adhesion properties not different SS-SS cohesion properties.

By comparison, SS showed the following rank order in terms of size: D_e (1.66 ± 0.06 μm) < D_{ae} (2.2 ± 0.2 μm) < MMAD (3.26 ± 0.18 μm). High MMAD values, in comparison to D_{ae}, value could be attributed to cohesion between SS particles in the dry powder state (Figure 6a) and the formation of FPA within SS-mannitol formulations (Figure 6c−f). GSD measurements of SS obtained from all formulations were around 2 (2.1 ± 0.0), which is indicative of polydisperse aerodynamic size distribution.

Comparing SS-CrM formulations demonstrated higher amounts of SS deposited on the throat (IP) in the case of CrM crystals with rougher surface (linear, r^2 = 0.8299) and higher $FPM_{<5\ \mu m}$ content (linear, r^2 = 0.8985) (Figure 10). This

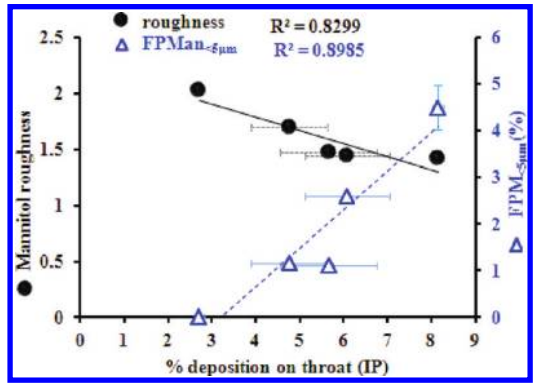

Figure 10. Amounts of salbutamol sulfate deposited on the throat (IP) (mean ± SD, $n \geq 3$) in relation to mannitol surface roughness (●) and fine particle mannitol ($FPM_{<5\ \mu m}$) (Δ).

could be explained by the "active sites" theory, as in the case of increased amounts of $FPM_{<5\ \mu m}$; they have higher possibility to occupy the active sites on mannitol surfaces leaving SS particles to agglomerate or to form SS-$FPM_{<5\ \mu m}$ aggregates (FPA) (Figure 6c−f) that have a higher probability to deposit on the throat by inertial impaction.

All formulations produced similar EM of SS (94.7 ± 1.3 − 96.3 ± 0.2%, $n \geq 3$, P > 0.05), which could be ascribed to similar flowability of all mannitol powders (section 3.5). Mannitol concentration used during crystallization was indirectly proportional to $FPF_{\leq 5\ \mu m}$ (linear, r^2 = 0.9887) and EI (linear, r^2 = 0.9948) but directly proportional to IL (linear, r^2 = 0.988) (Figure 11). This indicates that mannitol crystals grown from lower supersaturations can have better performance in DPI formulations containing salbutamol sulfate, as in theory, $FPF_{\leq 5\ \mu m}$ refers to the percentage fraction of the drug that is pharmacologically active.[34] The $FPF_{\leq 5\ \mu m}$ exhibited a decreasing trend (linear, r^2 = 0.9041) with increasing SS amounts remaining after 5 s of air jet sieving (Figure 12a). This relationship is important as it confirms that the enhanced aerosolization performance in the case of mannitol crystals grown from lower supersaturations was due to a lower degree of SS-mannitol adhesion forces.

As discussed previously, all formulations were prepared at the same blending conditions, contain the same batch of SS, and

dx.doi.org/10.1021/cg300224w | Cryst. Growth Des. 2012, 12, 3006−3017

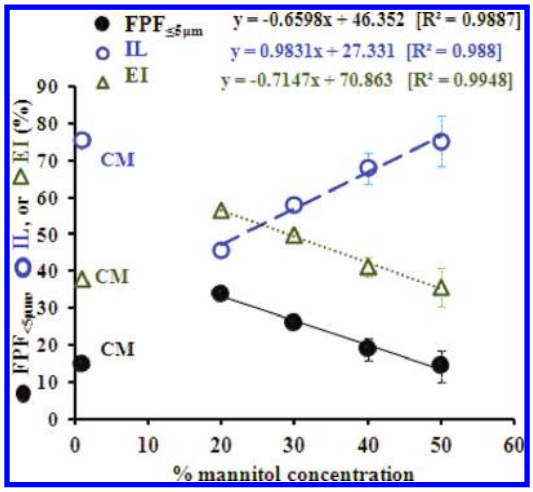

Figure 11. (●) Fine particle fraction ($FPF_{\leq 5\ \mu m}$), (○) impaction loss (IL), and (Δ) effective inhalation index (EI) (mean ± SD, $n \geq 3$) obtained from formulations containing different 63−90 μm sieved mannitol powders: commercial mannitol (CM) and cooling crystallized mannitol (CrM) from 20%, 30%, 40%, and 50% (w/v) solutions.

contain mannitol powders with similar flow properties, yet considerably different morphologies. Interestingly, a direct linear relationship (r^2 = 0.981) was established between mannitol AR/FR and $FPF_{\leq 5\ \mu m}$ (Figure 12b) demonstrating that carrier crystals with more elongated and less flattened habit produced better DPI performance. It is believed that more elongated/less flattened carrier particles will result in less drug-carrier contact points or less stable contact area[35,36] and thus fewer drug-carrier adhesion properties.[37] Also, elongated mannitol particles are expected to produce decreased press-on adhesive forces during the blending process (Figure 13). Furthermore, elongated mannitol crystals are expected to have more ability to stay airborne in an airflow (than isometric particles that have the same geometric size) and therefore they have more ability to travel further in lung airways. This will encourage SS particles to detach from the mannitol surface due to increased "effective" aerosolization time (Figure 13). Also, this concords with previous studies; correlations between $FPF_{\leq 5\ \mu m}$ with mannitol carrier physical properties showed direct linear relationships with $FPM_{<5\ \mu m}$ (r^2 = 0.9203),[38] (Figure 13b), SSA_v (r^2 = 0.9192),[6] D_{bulk} (r^2 = 0.906), and D_{tap} (r^2 = 0.8649) (Figure 13c).[7] Finally, it has to be noted that PSD, solid state, and in vitro inhalation performance for all mannitol samples and/or formulations were not profoundly affected when stored in sealed glass vials in ambient conditions for a minimum of 16 months (data not shown).

4. CONCLUSION

This study demonstrated that, controlled cooling crystallization of mannitol could be an attractive technique to allow the engineering of mannitol crystals with desired physicochemical properties and improved inhalation performance. The initial supersaturation degree used during crystallization of mannitol appears to be a critical factor in the control of the physicochemical properties. Mannitol crystals grown from low supersaturation grows as needle-like crystals whose length decreases linearly with increasing supersaturation. Furthermore, specific surface area, fine particles content, surface smoothness, bulk density, and tap density of mannitol crystals increase with decreasing supersaturation degree. Improved inhalation performance was obtained for formulations containing mannitol crystallized from lower supersaturations due to reduced salbutamol sulfate-mannitol adhesion. Mannitol crystals grown from 20% w/v solutions demonstrated the highest specific surface area, the highest fine particles content, the highest degree of shape elongation, and the smoothest surface topography produced the best DPI inhalation performance in terms of highest fine particle $fraction_{\leq 5\ \mu m}$ of 33.8 ± 1.2% compared to 14.9 ± 1.1% for the commercial grade. In this study, the crystallization work has been completed at a small scale and using uncontrolled cooling rates. Therefore, more crystallization development work would be valuable to fully determine the benefits of the cooling crystallization approach. Nevertheless, this study gives comparative information and highlights that mannitol crystal grown from low supersaturation would be desirable for DPI formulations, mainly due to their elongated habit, smoother surface, and higher "intrinsic" fines content.

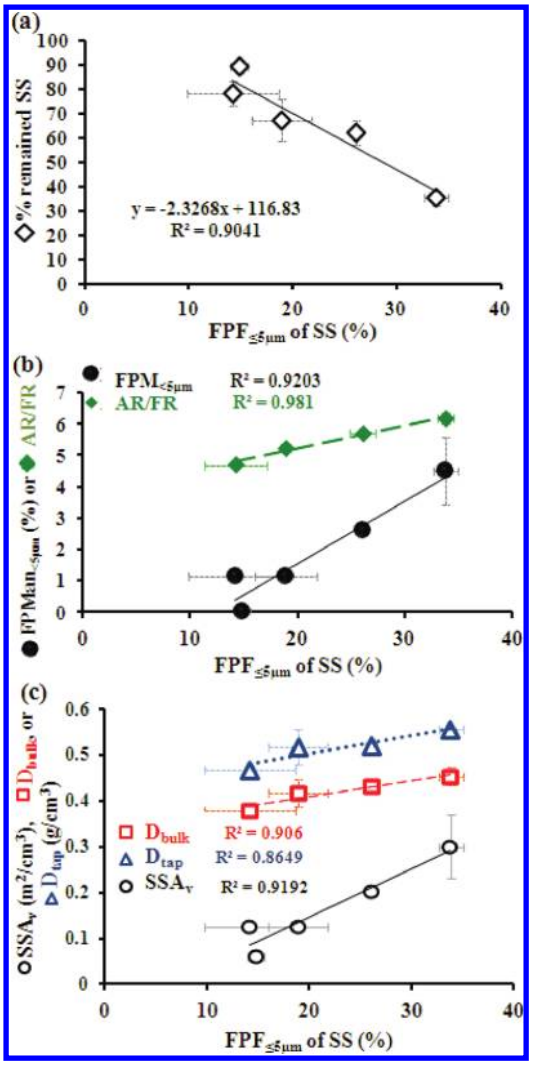

Figure 12. FPF of salbutamol sulfate (SS) in relation to (◊) % SS remained on the 45 μm sieve following 5 s air jet sieving (a), (●) fine particle mannitol ($FPM_{<5\ \mu m}$), (♦) aspect ratio/flatness ratio (AR/FR) (b), (□) bulk density (D_{bulk}), (Δ) tap density (D_{tap}), and (○) volume specific surface area (SSA_v) (c).

dx.doi.org/10.1021/cg300224w | Cryst. Growth Des. 2012, 12, 3006−3017

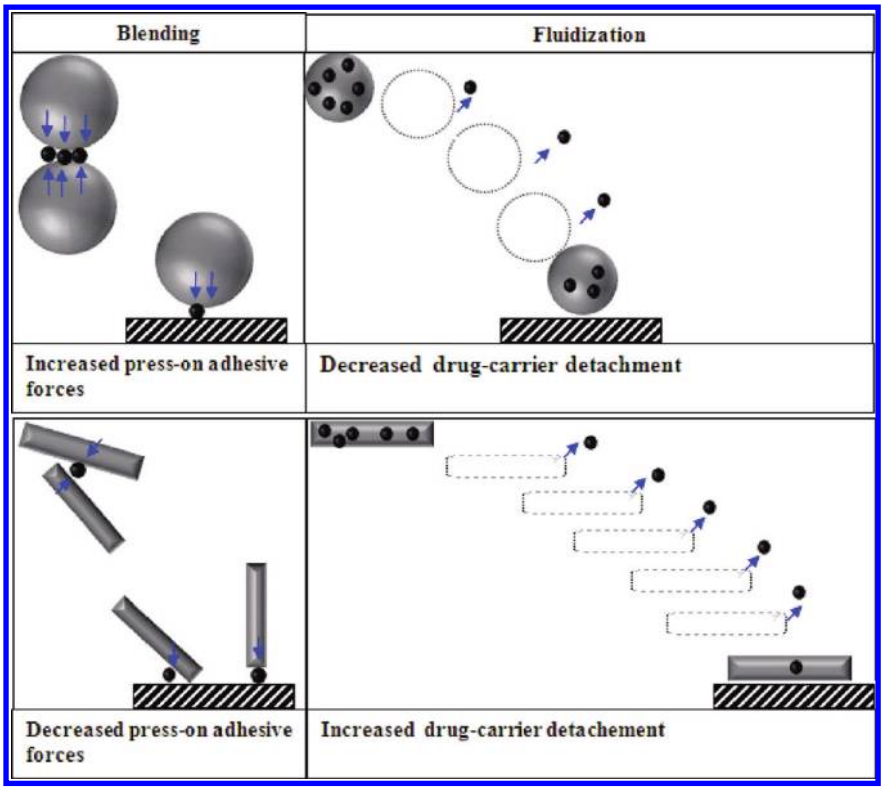

Figure 13. Schematic showing reduced drug-carrier adhesive forces and improved aerosolization efficiency for elongated carrier particles.

■ ASSOCIATED CONTENT

Supporting Information

Micromeritics properties of engineered mannitol in detail (Carr's ndex, porosity, and span) and DSC traces. This information is available free of charge via the Internet at http://pubs.acs.org/

■ AUTHOR INFORMATION

Corresponding Author

*Tel: +44 1634 202947. E-mail: a.nokhodchi@kent.ac.uk (A.N.). Email: waseemkaialy@hotmail.co.uk (W.K.).

Notes

The authors declare no competing financial interest.

■ ACKNOWLEDGMENTS

W.K. thanks Mr. Ian Slipper (School of Science, University of Greenwich) for SEM images.

■ REFERENCES

(1) Grossman, J. *J. Asthma* **1994**, *31*, 55−64.
(2) Telko, M. J.; Hickey, A J. *Respir. Care* **2005**, *50*, 1209−1222.
(3) Davis., S. S. *Pharm. Sci. Technol. Today* **1999**, *2*, 450−456.
(4) Ashurst, I.; Malton, A.; Prime, D.; Sumby, B. *Pharm. Sci. Technol. Today* **2000**, *3*, 246−256.
(5) Newman, S. P.; Moren, F.; Trofast, E.; Talaee, N.; Clarke, S. W. *Eur. Respir. J.* **1989**, *2*, 247−252.
(6) Kaialy, W.; Martin, G. P.; Ticehurst, M. D.; Momin, M. N.; Nokhodchi, A. *Int. J. Pharm.* **2010**, *392*, 178−188.
(7) Kaialy, W.; Martin, G. P.; Ticehurst, M. D.; Royall, P.; Mohammad, M. A.; Murphy, J.; Nokhodchi, A. *AAPS J.* **2011**, *13*, 30−43.
(8) Steckel, H.; Müller, B. W. *Int. J. Pharm.* **1997**, *154*, 19−29.
(9) Karhu, M.; Kuikka, J.; Kauppinen, T.; Bergström, K.; Vidgren, M. *Int. J. Pharm.* **2000**, *196*, 95−103.
(10) Kaialy, W.; Martin, G. P.; Larhrib, H.; Ticehurst, M. D.; Kolosionek, E.; Nokhodchi, A. *Colloid. Surface B* **2012**, 29−39.
(11) Mackin, L. A.; Rowley, G.; Fletcher, E. J. *Pharm. Sci.* **1997**, *3*, 583−586.
(12) Kaialy, W.; Momin, M. N.; Ticehurst, M. D.; Murphy, J.; Nokhodchi, A. *Colloid. Surfaces B* **2010**, *79*, 345−356.
(13) Kaialy, W.; Ticehurst, M. D.; Murphy, J.; Nokhodchi, A. *J. Pharm. Sci.* **2011**, *100*, 2665−2684.
(14) Ikegami, K.; Kawashima, Y.; Takeuchi, H.; Yamamoto, H.; Isshiki, N.; Momose, D.; Ouchi, K. *Pharm. Res.* **2002**, *19*, 1439−1445.
(15) Kaialy, W.; Alhalaweh, A.; Velaga, S. P.; Nokhodchi, A. *Int. J. Pharm.* **2011**, *412*, 12−23.
(16) Begat, P.; Morton, D. A. V.; Staniforth, J. N.; Price, R.. *Pharm. Res.* **2004**, *21*, 1591−1597.
(17) Mullin, J. W. *Crystallization*; Butterworth-Heinemann: Oxford, 1992.
(18) Janoo, V. *Quantification of Shape, Angularity, and Surface Texture of Base Course Materials*; Special Report 98-1; U. S. Army Corps of Engineers: Hanover, New Hampshire, 1998; pp 2−17.
(19) Danish, F. Q.; Parrott, E. L. *J. Pharm. Sci.* **1971**, *60*, 548−554.
(20) Braatz, R. D. *Annu. Rev. Control* **2002**, *26*, 87−99.
(21) Kapil, V.; Dodeja, A. K.; Sarma, S. C. *J. Food Sci. Technol.* **1991**, *28*, 167−170.
(22) Brito, A. B. N.; Giulietti, M. *Cryst. Res. Technol.* **2007**, *42*, 583−588.
(23) Henisch, H. Cambridge University Press: Cambridge, U.K., 1988.
(24) Diepen, P. J. Thesis, Delft University of Technology, 1998.
(25) Yu, L.; Mishra, D. S.; Rigsbee, D. R.. *J. Pharm. Sci.* **1998**, *87*, 774−777.
(26) Burger, A.; Henck, J. O.; Hetz, S.; Rollinger, J. M.; Weissnicht, A. A.; Stöttner, H. *J. Pharm. Sci.* **2000**, *89*, 457−468.
(27) Dhumal, R. S.; Biradar, S. V.; Paradkar, A. R.; York, P. *Int. J. Pharm.* **2009**, *368*, 129−37.
(28) Kachrimanis, K.; Nikolakakis, I.; Malamataris, S. *J. Pharm. Sci.* **2000**, *89*, 250−259.

(29) Koivisto, M.; Suihko, E.; Lehto, V. P. *Z. Kristallogr. Suppl.* **2006**, *23*, 563−568.
(30) Yang, G.; Kubota, N.; Sha, Z.; Louhi-Kultanen, M.; Wang, J. *Cryst. Growth. Des.* **2006**, *6*, 2799−2803.
(31) Ban, S.; Hasegawa, J. *Biomaterials* **2002**, *23*, 2965−2972.
(32) Zhang, H. G.; Zhu, Q.; Wang, Y. *Chem. Mater.* **2005**, *17*, 5824−5830.
(33) Labiris, N. R.; Dolovich, M. B. *Br. J. Clin. Pharmacol.* **2003**, *56*, 588−599.
(34) Dunbar, C. A.; Hickey, A. J.; Holzner, P. *Kona* **1998**, *16*, 7−45.
(35) Otsuka, A.; Iida, K.; Danjo, K.; Sunada, H. *Chem. Pharm. Bull.* **1988**, *36*, 741−749.
(36) Kaialy, W.; Ticehurst, M; Nokhodchi, A. *Int. J. Pharm.* **2012**, *423*, 184−194.
(37) Hooton, J. C.; German, C. S.; Allen, S.; Davies, M. C.; Roberts, C. J.; Tendler, S. J. B.; Williams, P. M. *Pharm. Res.* **2004**, *21*, 953−961.
(38) Islam, N.; Stewart, P.; Larson, I.; Hartley, P. *Pharm. Res.* **2004**, *21*, 492−499.